



# In situ LA-ICPMS U–Pb dating of sulfates: applicability of carbonate reference materials as matrix-matched standards

Aratz Beranoaguirre<sup>1,2,3,4</sup>, Iuliana Vasiliev<sup>5</sup>, and Axel Gerdes<sup>2,3</sup>

<sup>1</sup>Institut für Angewandte Geowissenschaften, Karlsruher Institut für Technologie, Adenauerring 20b, 76131 Karlsruhe, Germany

<sup>2</sup>Institut für Geowissenschaften, Goethe-Universität Frankfurt, Altenhöferallee 1, 60438 Frankfurt am Main, Germany

<sup>3</sup>Frankfurt Isotope and Element Research Center (FIERCE), Goethe-Universität Frankfurt, 60438 Frankfurt am Main, Germany

<sup>4</sup>Geologia Saila, Euskal Herriko Unibertsitatea UPV/EHU, Sarriena z/g, 48940 Leioa, Spain

<sup>5</sup>Senckenberg Biodiversity and Climate Research Centre (BiK-F), Senckenberganlage 25, 60325 Frankfurt am Main, Germany

**Correspondence:** Aratz Beranoaguirre (aratz.beranoaguirre@kit.edu)

Received: 18 March 2022 – Discussion started: 1 April 2022

Revised: 2 August 2022 – Accepted: 11 August 2022 – Published: 6 September 2022

**Abstract.** Recent developments in analytical capabilities in the field of in situ laser ablation mass spectrometry (LA-ICPMS) have expanded the applications of U–Pb geochronometers in low-U minerals such as carbonates or garnets. The rapid evolution of the technique relies on well-characterized matrix-matched reference materials. In this article, we explore the suitability of using carbonate as an “almost-matrix-matched reference material” for in situ U–Pb dating of sulfates. For such purpose, we have used the astrochronologically dated gypsum and anhydrite samples deposited during the Messinian Salinity Crisis (5.97–5.33 Ma) and compared these dates with the U–Pb ages obtained by LA-ICPMS. Although the majority of the samples failed due to the elevated common Pb content and low  $^{238}\text{U}/^{204}\text{Pb}$  ratios, five of the samples showed a higher dispersion on U/Pb ratios. The obtained dates in four of these samples are comparable with the expected ages, while another gave an unexpected younger age, each of them with 6%–11% of uncertainty. The pit depth of the spots showed that the sulfates ablate similar to carbonates, so the offset due to the crater geometry mismatch or downhole fractionation can be assumed to be negligible. To sum up, the bias between the U–Pb and expected cyclostratigraphic ages, if any, is included in the uncertainty, and thus the results obtained here suggest that carbonate reference material is currently the best option for standardization of in situ U–Pb sulfate analyses.

## 1 Introduction

Recent developments in instrumentation and analytical capabilities of LA-ICPMS techniques have greatly expanded the applicability of the U–Pb geochronometer. The high spatial resolution, low cost of analysis and high throughput with relatively good precision (Schaltegger et al., 2015) achievable with the new generation of laser and mass spectrometers favour the study of minerals with low and heterogeneous U concentrations like carbonates or garnets (e.g. Roberts et al., 2020). In fact, carbonate geochronology has gone from scarce publications that involve tedious and long-lasting isotope dilution techniques (e.g. Brannon et al., 1996; Grandia et al., 2000; Woodhead et al., 2006, 2012; Rasbury and Cole, 2009) to a bloom of dozens of publications per year (extensive review in Roberts et al., 2020). Likewise, garnet U–Pb dating is rapidly developing in skarn and metamorphic garnets, with U contents even below 100 ppb (e.g. Burisch et al., 2019; Yan et al., 2020; Millonig et al., 2020). In addition, several laboratories have started to investigate the possibility of measuring other types of minerals: dolomites (Burisch et al., 2017), fluorite (Piccione et al., 2019; Lenoir et al., 2021), nacrite (Piccione et al., 2019) and anatase (Sindern et al., 2019), among others.

The rapid evolution of U–Pb dating in low-U phases is closely related to the availability of reference materials (WC-1 carbonate, Roberts et al., 2017; Mali garnet, Seman et

al., 2017). Well-characterized matrix-matched reference material is essential for U–Pb analyses by ion probe or laser ablation as the sample matrix affects the ablation, transport and ionization (Sylvester, 2008; Yang et al., 2018). Indeed, LA-ICPMS dates could only be as good as the homogeneity of the reference materials and the accuracy and precision to which such material is known (Schaltegger et al., 2015). Several authors, however, have appraised the suitability of using non-matrix-matched standardization with different levels of success. Deng et al. (2017) and Wafforn et al. (2018) used 91 500 and GJ1 zircon, respectively, to correct U/Pb fractionation of garnet and assumed they obtained the correct ages, whereas Yang et al. (2018) measured garnet ages 11 % too old using zircon standardization. Similarly, Parrish et al. (2018) measured Mud Tank zircon within carbonate analyses and reported a bias between zircon and calcite of ca. 4.7 %. Piccione et al. (2019) used the WC-1 carbonate reference material for fluorite analysis assuming that the bias between calcite and fluorite may likely be less than the one between calcite and zircon.

This study aims to continue opening new possibilities in the field of in situ U–Pb dating of low-U minerals by (i) demonstrating that sulfates can be dated by U–Pb and (ii) examining the suitability and reliability of using calcite as an “almost matrix-matched reference material” for sulfates. Accurate U–Pb dating of sulfates could contribute to a better understanding of their formation and/or transformation (hydration–dehydration) with the potential of dating diagenetic, pedogenic or tectonic processes. Gypsum ( $\text{CaSO}_4 \cdot 2\text{H}_2\text{O}$ ) and anhydrite ( $\text{CaSO}_4$ ) are the two most abundant sulfates of marine and non-marine evaporite deposits (e.g. Murray, 1964; Babel and Schreiber, 2014). Sedimentary gypsum forms by direct precipitation out of water evaporation under arid climatic conditions in hydrologically restricted environments. Under terrestrial evaporitic conditions, gypsum is the dominant primary mineral, and anhydrite forms through gypsum dehydration caused during diagenesis. In the presence of water at shallower levels, the anhydrite is rapidly converted back to gypsum (e.g. Conley and Bundy, 1958; Murray, 1964; Ossorio et al., 2014; Warren, 2016). Although less frequent, non-evaporitic gypsum formation can also take place (see Van Driessche et al., 2019, and references therein).

In the absence of sulfate matrix-matched reference material, we have assumed that the bias between calcite and sulfate is smaller than with the other available reference materials. Both minerals behave very similarly during ablation (e.g. drill speed, U/Pb downhole fractionation) and ionization in the plasma ( $\text{Ca}^{2+}$  as the main cation). For evaluating the suitability of the calcite-based corrections, we have analysed gypsum and anhydrite samples from the Messinian Salinity Crisis (MSC) in the Mediterranean Sea (Roveri et al., 2014a, b; Vasiliev et al., 2017; Grothe et al., 2020; Andreetto et al., 2021) and compared them with their astrochronological data (calibrated with astronomically tuned timescales, such as Milankovic cycles, Laskar, 1999).

Chronostratigraphy of late Miocene to early Pliocene within the MSC is well constrained (CIESM, 2008; Manzi et al., 2013; Roveri et al., 2014a) and thus makes those samples ideal for comparison purposes.

## 2 Geological background

The Messinian Salinity Crisis (MSC, 5.97–5.33 Ma) successions record extreme fluctuations in the Mediterranean’s palaeoceanographic and environmental conditions (e.g. Hsü et al., 1973; Krijgsman et al., 1999; Manzi et al., 2013). At the end of the Miocene, the Mediterranean’s connections with the Atlantic Ocean were extremely reduced (e.g. Flecker et al., 2015; Krijgsman et al., 2018), whereas the freshwater supply from the eastern Paratethys increased (Flecker and Ellam, 2006; Krijgsman et al., 2010). Those palaeoceanographic changes led to the formation of hypersaline water bodies and the deposition of a kilometre-thick evaporite unit (Fig. 1a) (Ryan, 2009). The original definition of the MSC referred to a marked environmental change at the base of the Tripoli diatomite formation (Sicily, Italy) close to the Tortonian–Messinian boundary (Selli, 1960). Astronomical tuning of the pre-evaporitic succession showed that the MSC onset was synchronous throughout the Mediterranean (e.g. Krijgsman et al., 1999; Manzi et al., 2018; Meilijson et al., 2018). According to the shallow water–deep basin model (Hsü et al., 1973; Roveri et al., 2014a), evaporite precipitation was associated with a sea level drop in the range of 1500 m up to the almost complete desiccation of the Mediterranean, culminating in halite precipitation and marked by the incisions of deep canyons at the Mediterranean margins. However, a non-evaporitic gypsum formation during MSC has been also described (Hsü et al., 1978). Isotope analyses of gypsum hydration water and the salinity of fluid inclusions in MSC gypsum indicate large freshwater inputs during gypsum formation (Natalicchio et al., 2014; Evans et al., 2015; Costanzo et al., 2019). Additionally, suggestions of the important role of sulfur-oxidizing bacteria in biogeochemically mediated gypsum formation (Grothe et al., 2020) are increasingly used to explain low salinity yet high concentrations of  $\text{Ca}^{2+}$  and  $\text{SO}_4^{4-}$  (Clauer et al., 2000), during the formation of MSC evaporites.

According to previous publications (Roveri et al., 2008a, b, 2014a), the MSC can be separated into three main stages (Fig. 1b). Stage I (5.97–5.60 Ma), the so-called Primary Lower Gypsum (PLG, Lugli et al., 2010), is defined by the deposition of primary selenite gypsum unit. During stage II (5.60–5.55 Ma), large evaporite deposits occurred (Resedimented Lower Gypsum unit, RLG), which includes halite, gypsum cumulates and brecciated limestones (Calcare di Base type 3, Manzi et al., 2011). Likewise, clastic gypsum derived from the dismantlement of the PLG unit can be found within this stage. Finally, alternating gypsum (mainly bottom grown selenite and cumulate) and

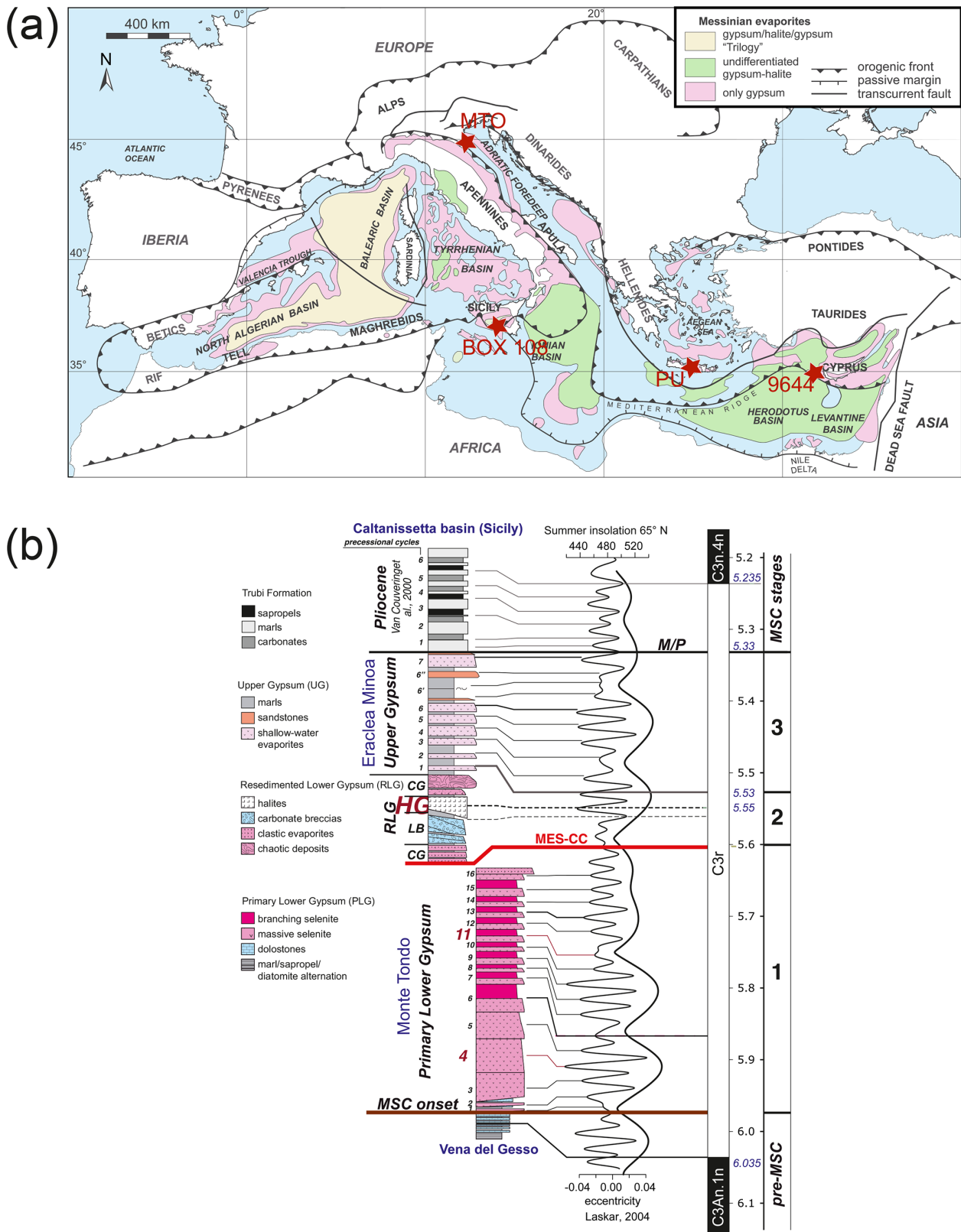


**Figure 1.** (a) Geological sketch of the Messinian evaporite deposits along the Mediterranean Sea (modified after Rouchy and Caruso, 2006). Note that only the successfully dated sample locations are shown. (b) Chronostratigraphy of late Miocene to early Pliocene with MSC events in the Mediterranean (modified from Vasiliev et al., 2017).

fine- to coarse-grained terrigenous deposits form the Upper Gypsum unit (UG, stage III, 5.55–5.33 Ma). There is no outcrop with the complete section of the MSC, but different segments are well exposed throughout the Mediterranean.

### 3 Methodology

U–Pb data were acquired in situ in polished mounts and slabs using a RESOLution 193 nm ArF excimer laser (CompeXPro 102) equipped with a two-volume ablation cell (Laurin Technic S155) coupled to a (i) single collector (SC) ICPMS (ElementXR, Thermo Scientific) or (ii) multi-collector (MC) ICPMS (Neptune Plus, Thermo Scientific) at FIERCE (Frankfurt Isotope & Element Research Center), Goethe University Frankfurt. The method is modified after Ring and Gerdes (2016) and Burisch et al. (2017). Samples are pre-screened in order to identify sub-zones with a higher  $^{238}\text{U}/^{206}\text{Pb}$  ratio before each analytical session.

The first sessions, between December 2019 and May 2020, were performed with the SC-ICPMS. Prior to the measurements, signal strength was tuned for maximum sensitivity while keeping oxide formation below  $\sim 0.5\%$  (UO/U) and element fraction low (e.g. Th/U  $\sim 0.9$ ). This was done by ablating at  $3\ \mu\text{m s}^{-1}$  with a  $60\ \mu\text{m}$  spot at 6 Hz and  $3.5\ \text{J cm}^{-2}$  fluence in the glass SRMNIST 612 (Jochum et al., 2011). The average sensitivity obtained for the line is ca. 100 000 cps per  $\mu\text{g g}^{-1}$  for  $^{238}\text{U}$ . The detection limits ( $4\times$  background signal) of the instrument for  $^{206}\text{Pb}$  and  $^{238}\text{U}$  were ca. 0.3 and  $0.03\ \text{ng g}^{-1}$ . Data were acquired in fully automated mode overnight. Each analysis consists of 18 s background acquisition followed by 18 s of sample ablation and 20 s washout. During 36 s data acquisition, the signals of  $^{206}\text{Pb}$ ,  $^{207}\text{Pb}$ ,  $^{208}\text{Pb}$ ,  $^{232}\text{Th}$  and  $^{238}\text{U}$  were detected by peak jumping in simultaneous analogue and pulse-counting mode. Detailed data acquisition parameters are summarized in Table 1.

Due to the low precision obtained in those sessions, with only two samples from a single session being considered acceptable (see results and discussion), the use of the more sensitive MC-ICPMS (Craig et al., 2018, 2020) was deemed necessary for subsequent measurements. The sessions with the MC-ICPMS were carried out between July 2020 and December 2020. As for the single collector, signal strength was tuned for maximum sensitivity while keeping oxide formation below  $\sim 0.5\%$  (UO/U) and element fraction low (e.g. Th/U  $\sim 0.9$ ). In that case, it was done with a  $35\ \mu\text{m}$ , 6 Hz, ca.  $3.5\ \text{J cm}^{-2}$  fluence and a  $3\ \mu\text{m s}^{-1}$  line ablated in the glass SRMNIST 614 (Jochum et al., 2011). The average sensitivity obtained for the line is ca. 120 000 cps per  $\mu\text{g g}^{-1}$  for  $^{238}\text{U}$  (note the smaller spot size compare to the SC-ICPMS). The detection limits in the multi-collector ICPMS were ca. 0.3 and  $0.01\ \text{ng g}^{-1}$  for  $^{206}\text{Pb}$  and  $^{238}\text{U}$ , respectively. The analyses were done during 31 s (15 s background and 16 s of ablation) in static mode, measuring  $^{206}\text{Pb}$  and  $^{207}\text{Pb}$  with secondary electron multipliers (SEMs),  $^{202}\text{Hg}$  and  $^{204}\text{Pb}$  with

multiple ion counters (MICs), and  $^{232}\text{Th}$  and  $^{238}\text{U}$  on Faraday cups with  $10^{13}\ \Omega$  amplifiers. Faraday signals in V are converted into counts per second (cps) by using a factor of 62 400 000. Detailed data acquisition parameters are summarized in Table 2.

In each analytical session, soda–lime glass SRMNIST614 was used as the primary reference material to correct for mass bias ( $^{207}\text{Pb}/^{206}\text{Pb}$ ) and the interelement fractionation and instrumental drift ( $^{206}\text{Pb}/^{238}\text{U}$ ) throughout the entire analytical session. Carbonate reference material WC-1 (254 Ma, Roberts et al., 2017) was used to determine the difference of the Pb/U fractionation between carbonate and synthetic glass matrix. Depending on the analytical conditions (i.e. spot size, laser fluence, torch position, sample gas flows) the matrix effect can vary up to 12 % (FIERCE laboratory observation; e.g. Cruset et al., 2021), and even at similar tuning parameters, two sessions separated by some weeks could result in different Pb–U correction factors. So far, this behaviour is not very well understood, and due to its unpredictability, the matrix correction is calculated for each session (see below). Secondary reference calcite materials, ASH-15D calcite ( $2.965 \pm 0.011$  Ma, Nuriel et al., 2021), B-6 ( $42.99 \pm 0.99$  Ma, only LA-ICPMS data, Pagel et al., 2018) and in-house calcite (reproducible age of ca. 36 Ma) were measured for quality control. Not all the secondary reference materials were used in each session (see information in Tables 1 and 2).

Raw data were corrected offline using an in-house VBA spreadsheet programme (Gerdes and Zeh, 2006, 2009). Following background and interferences corrections, outliers ( $\pm 2\sigma$ ) were rejected based on the time-resolved  $^{207}\text{Pb}/^{206}\text{Pb}$  and  $^{206}\text{Pb}/^{238}\text{U}$  ratios as well as the Pb and U signal. All in all, five sessions were performed, and the matrix Pb/U correction factors (carbonate vs SRMNIST glass) applied to each of them are as follows: 4.5 % for SC-ICPMS session, 8 % for MC-ICPMS session 1 (same spot size for both carbonate and SRMNIST glass, see Table 2), 0.5 % for session 2 (different spot size, Table 2), 0 % for session 3 and 0 % for session 4. The  $^{206}\text{Pb}/^{238}\text{U}$  downhole fractionation during 16 and 18 s depth profiling was estimated to be 3 % based on the common-Pb-corrected WC-1 analyses and was applied as an external correction to all sulfate analyses and secondary reference materials. Uncertainties for each isotopic ratio are the quadratic addition of the within-run precision, counting statistic uncertainties of each isotope, and the excess of scatter and variance (Horstwood et al., 2016) calculated from the SRMNIST 614 and the WC-1 after drift correction. To account for the long-term reproducibility of the method we added by quadratic addition an expanded uncertainty of 1.5 % to the final age of all analysed samples (Montano et al., 2021). This was deducted from repeated analyses of ASH-15D in the FIERCE laboratory between 2017 and 2019. Data were displayed in Tera–Wasserburg plots and ages were calculated as lower concordia curve intercepts using the same algorithms as Isoplot 4.15 (Ludwig, 2012). All

**Table 1.** LA-SC-ICPMS U–Pb analysis procedure at Goethe University Frankfurt, FIERCE laboratory.

Laboratory and sample preparation	
Laboratory name	FIERCE, Frankfurt Isotope & Element Research Center Goethe Universität, Frankfurt am Main
Sample type/mineral	Sulfate
Sample preparation	25 mm polished resin mounts
Imaging	Petrographic microscope and 2400 dpi digital scan
Laser ablation system	
Make, model and type	RESOLution ArF excimer laser (COMPex Pro 102)
Ablation cell	Two-volume ablation cell (Laurin Technic S155)
Laser wavelength	193 nm
Pulse width	20 ns
Fluence	2 J cm <sup>-2</sup>
Repetition rate	10 Hz
Pre-ablation	4 pulses (same parameters as main ablation)
Ablation duration	18 s
Ablation rate	~ 0.6 μm s <sup>-1</sup> (in the primary RM), ~ 0.9 μm s <sup>-1</sup> (in carbonate and sulfate)
Spot shape and size	Round, 154 μm (diameter)
Sampling mode	Static spot ablation
Gases	Sample cell: He. Funnel: He + Ar. Tubbing: He + Ar + N <sub>2</sub>
Gas flows	He (300 mL min <sup>-1</sup> ), Ar (1050 mL min <sup>-1</sup> ), N <sub>2</sub> (8 mL min <sup>-1</sup> ).
ICP-MS instrument	
Make, model and type	Thermo Scientific ElementXR sector field ICP-MS
Sample introduction	Ablation aerosol
RF power	1300 W
Detection system	Secondary electron multiplier (with conversion dynode at –8 kV). Simultaneous analogue and counting (pulse) modes of detection (conversion factors calculated per mass and applied offline). Magnetic field fixed. Detection by peak jumping with electrostatic analyser.
Masses measured	206, 207, 232, 238
Dwell times	206: 6.4 ms, 207: 7.5 ms, 232: 2.0 ms, 238: 4.6 ms
Samples per peak/integration type	4 for all masses/average
Total time per run	99 ms
Number of runs/total time	370/36.6 s
Acquisition mode	Trigger from laser (20 s after pre-ablation), background: 18 s, ablation: 18 s
Dead time	29 ns
Data processing	
Gas blank	20 s on-peak zero subtracted.
Calibration strategy	SRMNIST614 as primary RM, WC-1 as offset RM, and ASH15D as validation RM.
Reference material (RM) information	Soda–lime glass SRMNIST614 (Jochum et al., 2011), WC-1 (Roberts et al., 2017), ASH15D (Nuriel et al., 2021)

Table 1. Continued.

Data processing	
Data processing/LIEF correction	In-house VBA spreadsheet programme (Gerdes and Zeh, 2006, 2009). Intercept method for LIEF correction, assumes Pbc-corrected WC-1 and samples behave identically.
Mass discrimination	$^{207}\text{Pb}/^{206}\text{Pb}$ (0.2 %) and $^{206}\text{Pb}/^{238}\text{U}$ (5 %) normalized to primary standard
Common Pb correction	No common Pb correction applied to the data.
Uncertainty level and propagation	Uncertainties are quoted at $2\sigma$ absolute and are propagated by quadratic addition of the within run precision (SD of the mean of ratios in log-ratio space), counting statistics, background, common Pb correction (if applicable) and the excess of scatter (calculated from the primary RM). In addition, an excess of variance of 1.45 % ( $1\sigma$ ), calculated from the offset RM, was added quadratically to the $^{206}\text{Pb}/^{238}\text{U}$ ratios. Systematic uncertainties are reported as an expanded uncertainty, considering long-term reproducibility (1.5 %, $2\sigma$ ) and decay constant uncertainties.
Quality control/validation	WC-1: $254.7 \pm 2.3/4.4$ Ma (2 s, MSWD = 1.00, $n = 28$ ) ASH15D: $3.004 \pm 0.153/0.159$ Ma (2 s, MSWD = 0.85, $n = 28$ ) (Ages are the $^{206}\text{Pb}/^{238}\text{U}$ lower intercept ages of the calculated isochrons with the concordia curve in the Tera–Wasserburg space)

uncertainties are reported at the  $2\sigma$  level. After the analysis, the depth of the ablation pit was measured in several spots per sample, including the WC-1 and SRM NIST 614 reference materials, using the Keyence VHX 6000 digital microscope.

## 4 Samples and results

### 4.1 U–Pb dating

U–Pb dating was applied to 32 samples from the different locations and all available gypsum–anhydrite varieties (large selenite crystals, banded selenite, gypsum cumulates, anhydrite, halite with gypsum and anhydrite intercalation) across the Mediterranean Sea (Fig. 1), which display variable contents of Pb and U. Only five of them were successfully dated (15 % of success). The undatable samples are characterized by analyses that clustered near the common Pb intercept, disclosing a large amount of common Pb (Fig. 2). This low  $\mu$  ( $^{238}\text{U}/^{204}\text{Pb}$  ratio) makes it impossible to draw any regression line. No link between successful and unsuccessful samples or their texture could be established, and both successful and unsuccessful samples were found within the same type of gypsum. The successfully dated samples are described below, and their results are presented in Fig. 3 as well as in Tables S1 and S2 in the Supplement.

#### 4.1.1 Sample MTO 4-4

The MTO 4-4 sample was collected at the Monte Tondo gypsum quarry, located within the Vena del Gesso basin (along the western Romagna Apennines), and belongs to the PLG (Lugli et al., 2007, 2010; Vasiliev et al., 2017). It is a banded selenite (type F4 of Lugli et al., 2010), and the cyclostrati-

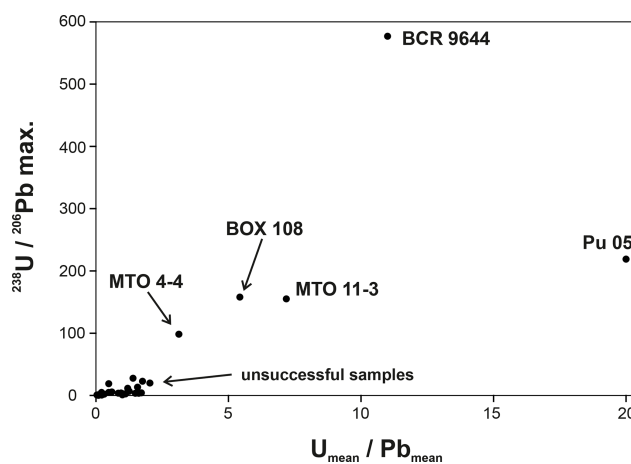


Figure 2. Diagram showing  $U_{\text{mean}}$  content to  $Pb_{\text{mean}}$  content vs. maximum value on the  $^{238}\text{U}/^{206}\text{Pb}$  axis. The successfully dated samples have a distinctively higher U/Pb heterogeneity.

graphic age is 5.92 Ma, which is close to the onset of the MSC. The sample was measured in three different sessions. The maximum U and Pb contents on the analysed spots are 2.34 and  $3.85 \mu\text{g g}^{-1}$ , respectively, depicting a maximum U/Pb ratio of 98.4 in the best case. The first of the sessions was measured with the SC-ICPMS and the analyses define a regression line with a lower intercept at  $6.01 \pm 1.19$  Ma ( $\pm 2\sigma$ , MSWD = 1.07, Fig. 3). The other two sessions were measured with the MC-ICPMS and the lower intercepts of the regression lines are  $5.55 \pm 0.61$  Ma ( $\pm 2\sigma$ , MSWD = 1.00, Fig. 3) and  $5.73 \pm 0.37$  Ma ( $\pm 2\sigma$ , MSWD = 1.13, Fig. 3).

**Table 2.** LA-MC-ICP-MS U–Pb analysis procedure at Goethe University Frankfurt, FIERCE laboratory.

Laboratory and sample preparation	
Laboratory name	FIERCE, Frankfurt Isotope & Element Research Center Goethe Univesität, Frankfurt am Main
Sample type/mineral	Sulfate
Sample preparation	25 mm polished resin mounts
Imaging	Petrographic microscope and 2400 dpi digital scan
Laser ablation system	
Make, model and type	RESOLution ArF excimer laser (COMPex Pro 102)
Ablation cell	Two-volume ablation cell (Laurin Technic S155)
Laser wavelength	193 nm
Pulse width	20 ns
Fluence	2 J cm <sup>-2</sup>
Repetition rate	10 Hz
Pre-ablation	2 pulses (same parameters as main ablation)
Ablation duration	16 s
Ablation rate	~ 0.6 μm s <sup>-1</sup> (in the primary RM), ~ 0.9 μm s <sup>-1</sup> (in carbonate and sulfate)
Spot shape and size	Round, 130 μm (75 μm for primary RM), except for session 1 (90 μm for all spots)
Sampling mode	Static spot ablation
Gases	Sample cell: He. Funnel: He + Ar. Tubbing: He + Ar + N <sub>2</sub>
Gas flows	He (300 mL min <sup>-1</sup> ), Ar (~ 950 mL min <sup>-1</sup> ), N <sub>2</sub> (5–10 mL min <sup>-1</sup> ). Ar and N <sub>2</sub> are tuned each session, so the values can be slightly different
ICP-MS instrument	
Make, model and type	Thermo Scientific Neptune Plus multi-collector ICP-MS
Sample introduction	Ablation aerosol
RF power	1300 W
Detection system	Simultaneous multi-collection. Secondary electron multipliers (SEMs) for <sup>206</sup> Pb and <sup>207</sup> Pb Multiple ion counters (MICs) for <sup>202</sup> Hg and <sup>204</sup> Pb Faraday cups with 10 <sup>13</sup> Ω amplifiers for <sup>232</sup> Th and <sup>238</sup> U
Masses measured	202, 204, 206, 207, 232, 238
Total time per run	131 ms
Number of runs/total time	230/30.1 s
Acquisition mode	Trigger from laser (14 s after pre-ablation), background: 15 s, ablation: 16 s
Dead time	29 ns
Data processing	
Gas blank	15 s on-peak zero subtracted.
Calibration strategy	SRMNIST614 as primary RM, WC-1 as offset RM, and ASH15D, B6 and in-house calcite as validation RM.
Reference material (RM) information	Soda–lime glass SRMNIST614 (Jochum et al., 2011), WC-1 (Roberts et al., 2017), ASH15D (Nuriel et al., 2021), B-6 (Pagel et al., 2018), CalBraun (in-house calcite RM)

Table 2. Continued.

Data processing	
Data processing/LIEF correction	In-house VBA spreadsheet programme (Gerdes and Zeh, 2006, 2009). Intercept method for LIEF correction, assumes Pbc-corrected WC-1 and samples behave identically.
Mass discrimination	$^{207}\text{Pb}/^{206}\text{Pb}$ and $^{206}\text{Pb}/^{238}\text{U}$ normalized to primary standard (variable in each session)
Common Pb correction	No common Pb correction applied to the data.
Uncertainty level and propagation	Uncertainties are quoted at $2\sigma$ absolute and are propagated by quadratic addition of the within-run precision (SD of the mean of ratios in log-ratio space), counting statistics, background, common Pb correction (if applicable) and the excess of scatter (calculated from the primary RM). In addition, an excess of variance calculated for each session from the offset RM, was added quadratically to the $^{206}\text{Pb}/^{238}\text{U}$ ratios. Systematic uncertainties are reported as an expanded uncertainty, considering long-term reproducibility (1.5 %, $2\sigma$ ) and decay constant uncertainties.
Quality control/validation	<p>Session 1:</p> <p>WC-1: <math>254.8 \pm 1.9/4.3</math> Ma (2 s, MSWD = 1.0, <math>n = 12</math>)            B-6: <math>42.73 \pm 0.59/0.87</math> Ma (2 s, MSWD = 0.84, <math>n = 12</math>)            CalBraun: <math>36.72 \pm 1.23/1.35</math> Ma (2 s, MSWD = 0.89, <math>n = 12</math>)</p> <p>Session 2:</p> <p>WC-1: <math>254.1 \pm 2.0/4.4</math> Ma (2 s, MSWD = 1.0, <math>n = 20</math>)            B-6: <math>42.66 \pm 0.47/0.80</math> Ma (2 s, MSWD = 0.50, <math>n = 22</math>)            CalBraun: <math>36.07 \pm 0.65/0.85</math> Ma (2 s, MSWD = 0.61, <math>n = 22</math>)</p> <p>Session 3:</p> <p>WC-1: <math>254.5 \pm 3.2/5.0</math> Ma (2 s, MSWD = 1.0, <math>n = 10</math>)            ASH15D: <math>3.060 \pm 0.193/0.198</math> Ma (2 s, MSWD = 1.0, <math>n = 10</math>)            B-6: <math>43.54 \pm 0.79/1.02</math> Ma (2 s, MSWD = 1.13, <math>n = 10</math>)</p> <p>Session 4:</p> <p>WC-1: <math>254.5 \pm 1.6/4.1</math> Ma (2 s, MSWD = 1.0, <math>n = 20</math>)            ASH15D: <math>3.091 \pm 0.102/0.112</math> Ma (2 s, MSWD = 0.88, <math>n = 20</math>)            B-6: <math>43.83 \pm 0.39/0.77</math> Ma (2 s, MSWD = 0.56, <math>n = 20</math>)            (Ages are the <math>^{206}\text{Pb}/^{238}\text{U}</math> lower intercept ages of the calculated isochrons with the concordia curve in the Tera–Wasserburg space. WC-1 RM are anchored at 0.85 value of <math>^{207}\text{Pb}/^{206}\text{Pb}</math>)</p>

#### 4.1.2 Sample MTO 11-3

This sample was also collected by Vasiliev et al. (2017) at the Monte Tondo gypsum quarry. It is a massive selenite (F3 of Lugli et al., 2010) and belongs to the younger cycles of the PLG. Its estimated cyclostratigraphic age is 5.701 Ma. MTO 11-3 was also measured in three different sessions. The maximum U and Pb content on the analysed spots are 5.49 and  $0.97 \mu\text{g g}^{-1}$ , respectively, depicting a maximum U/Pb ratio value of 155.2 in the best case. The first of the sessions was measured with the SC-ICPMS and the analyses define a regression line with a lower intercept at  $5.40 \pm 0.84$  Ma ( $\pm 2\sigma$ , MSWD = 1.13, Fig. 3). The other two sessions were measured with the MC-ICPMS and the lower intercepts of the regression lines are  $5.46 \pm 0.44$  Ma ( $\pm 2\sigma$ , MSWD = 1.41, Fig. 3) and  $5.55 \pm 0.32$  Ma ( $\pm 2\sigma$ , MSWD = 1.03, Fig. 3).

#### 4.1.3 Sample BOX 108

BOX 108 is a halite with anhydrite nodules. It comes from borehole EMS-4 (Cattolica Eraclea) in the Caltanissetta

Basin (southwest of Sicily) and was donated to Prof. Cita (University of Milano). The core was drilled from  $-82$  m to  $-665$  m below sea level, and the sample was located almost at the bottom (approximately at  $-610$  m). Cyclostratigraphic ages point to 5.55–5.60 Ma. The analyses were made in both halite and anhydrite, but only the anhydrite was successful. It was measured twice with the MC-ICPMS. The maximum U and Pb contents on the analysed spots are 5.70 and  $1.67 \mu\text{g g}^{-1}$ , respectively, depicting a maximum U/Pb ratio value of 158.0 in the best case. The analyses define a regression line with a lower intercept at  $5.55 \pm 0.35$  Ma ( $\pm 2\sigma$ , MSWD = 1.01, Fig. 3) in the first of the sessions and  $5.54 \pm 0.38$  Ma ( $\pm 2\sigma$ , MSWD = 1.49, Fig. 3) in the second.

#### 4.1.4 Sample BCR9644

Sample BCR9644 was collected from the cores of Deep Sea Drilling Program Site 42A hole 376 cored in 1975 west of Cyprus and stored at the Bremen International Ocean Drilling Program repository. BCR9644 was collected from a gypsum breccia at 170.28 m below sea level and has a

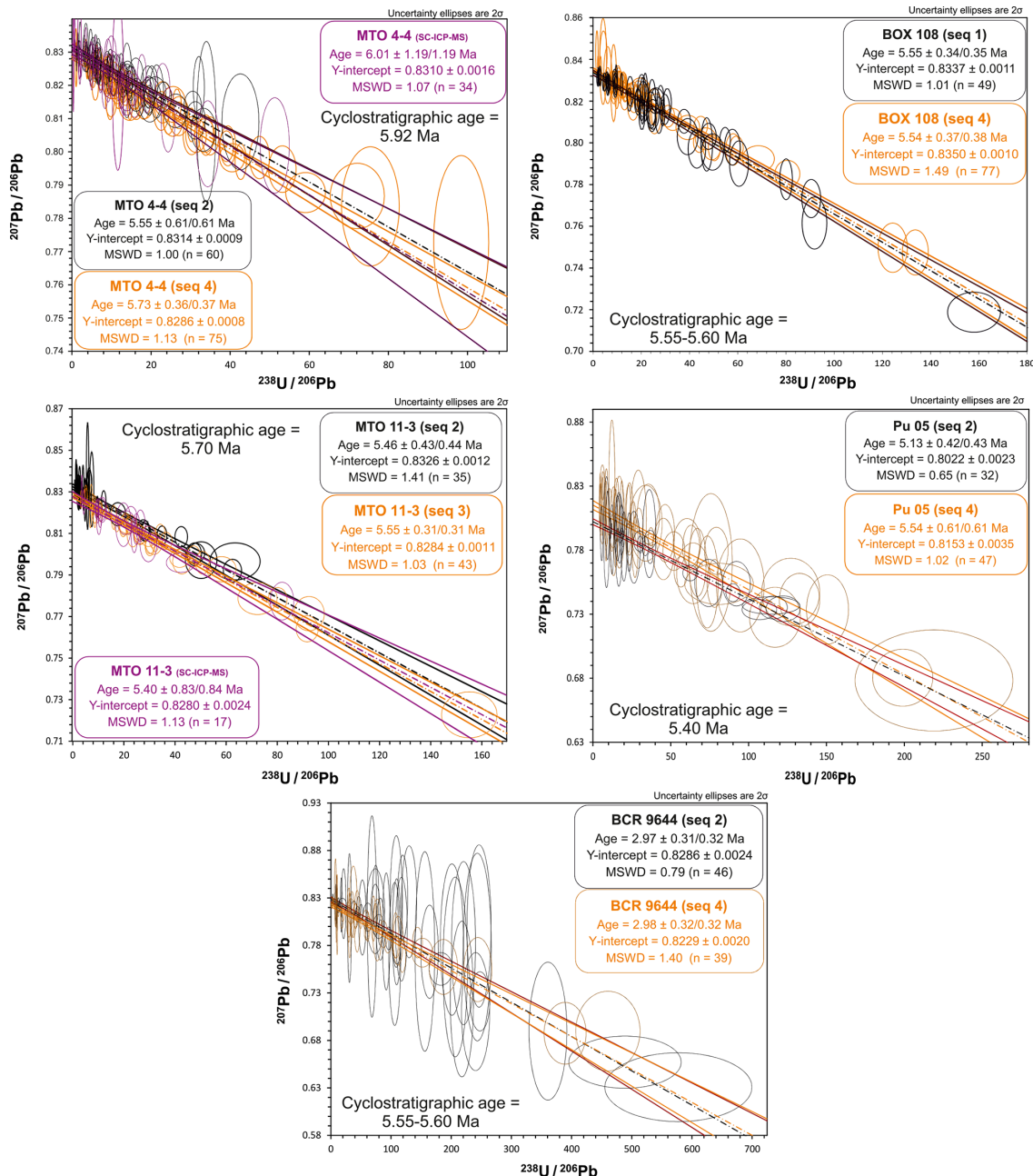


**Figure 3.** Tera–Wasserburg diagram ( $^{207}\text{Pb}/^{206}\text{Pb}$  vs.  $^{238}\text{U}/^{206}\text{Pb}$ ) for samples MTO 4-4, MTO 11-3, BOX 108, Pu 05 and BCR 9644. The blue ellipses and error envelope in samples MTO 4-4 and MTO 11-3 correspond to the analyses with the SC-ICPMS, while orange and black refer to two independent sessions with the MC-ICPMS. Both propagated within-session uncertainties and the expanded uncertainties are  $\pm 2\sigma$ .

stratigraphic age of ca. 5.55–5.60 Ma. It was measured twice with the MC-ICPMS. The maximum U and Pb contents on the analysed spots are 2.31 and  $0.61 \mu\text{g g}^{-1}$ , respectively, although Pb rarely exceeds  $0.1 \mu\text{g g}^{-1}$ . The maximum U/Pb ratio obtained in that sample is 577.5 in the best case. The low Pb contents imply large error ellipses, but successful regression lines have been defined, with a lower intercept at  $2.98 \pm 0.34 \text{ Ma}$  ( $\pm 2\sigma$ , MSWD = 0.79, Fig. 3) in the first

of the sessions and  $2.98 \pm 0.32 \text{ Ma}$  ( $\pm 2\sigma$ , MSWD = 1.40, Fig. 3) in the second.

#### 4.1.5 Sample Pu 05

This sample was collected in the Ploutis region (Central Crete, Greece), and it is a gypsum breccia. The stratigraphic age of these gypsum units is disputed as being part of the

PLG (Zachariasse et al., 2008), but the texture of direct capping by Lago Mare deposits strongly suggests that Pu 05 belongs to the UG unit. Its cyclostratigraphic age is ca. 5.40 Ma. Pu 05 was also measured twice with the MC-ICPMS. The maximum U and Pb contents on the analysed spots are 1.44 and  $0.16 \mu\text{g g}^{-1}$ , respectively, depicting a maximum U/Pb ratio value of 158.0 in the best case. Each session defines a regression line with a lower intercept at  $5.15 \pm 0.42 \text{ Ma}$  ( $\pm 2\sigma$ , MSWD = 0.68, Fig. 4) and  $5.54 \pm 0.61 \text{ Ma}$  ( $\pm 2\sigma$ , MSWD = 1.02, Fig. 4), respectively.

#### 4.2 Pit depth measurements

After the analyses, pit depths were measured in all the samples as well as in the carbonate reference materials. The measured pit depth averages were used for calculating the U and Pb contents (Tables S1 and S2). The shape and depth of the craters in WC-1 primary carbonate are all similar, and their average depth is  $15.0 \mu\text{m}$  ( $\text{SD} = 1.34$ ,  $n = 16$ ). Few spots corresponding to the secondary reference materials were also checked, and they are comparable to those of WC-1. The pits of the SRM NIST 614 are ca. 33 % shallower than the ones in the calcite matrix at around  $10 \mu\text{m}$  deep. Regarding the sulfate samples, the pit depth of samples MTO 4-4 and MTO 11-3 is rather homogeneous with mean values of  $29.6 \mu\text{m}$  ( $\text{SD} = 6.2$ ,  $n = 44$ ) and  $18.9 \mu\text{m}$  ( $\text{SD} = 5.9$ ,  $n = 37$ , Fig. 4a), respectively. Samples BCR 9644 and BOX 108 display zones with different heights in some of the ablation holes (Fig. 4b). Although they are exceptional, two ca.  $90 \mu\text{m}$  and two ca.  $60 \mu\text{m}$  pits were measured in BOX 108. Considering them, the average depth is  $28.2 \mu\text{m}$  ( $\text{SD} = 16.4$ ,  $n = 64$ ), whereas excluding those four heights the standard deviation improves substantially ( $25.0 \mu\text{m}$ ,  $\text{SD} = 8.8$ ,  $n = 60$ ). The average depth for sample BCR 9644 is  $16.2 \mu\text{m}$  ( $\text{SD} = 6.7$ ,  $n = 32$ ) excluding two ca.  $60 \mu\text{m}$  spots. On the other hand, sample PU 05 shows higher variability and larger standard deviation, since the pit depth varies from 29 to  $107 \mu\text{m}$ . The calculated average is  $62.6 \mu\text{m}$  ( $\text{SD} = 23.0$ ,  $n = 48$ ).

## 5 Discussion

### 5.1 Low success rate

#### 5.1.1 High common Pb content and potential applicability

The majority of the analysed samples, 27 out of 32, were unsuccessful due to the high common Pb content and hence low or non-existent spread in the  $^{238}\text{U}/^{206}\text{Pb}$  axis. Recent studies in the field of environmental hazards have shown that Pb tends to incorporate both gypsum and anhydrite into sulfates (Astilleros et al., 2010; Morales et al., 2014; Kameda et al., 2017). In fact, in the presence of high-Pb fluids, anglesite ( $\text{PbSO}_4$ ) is simultaneously intergrown with those sulfates. The behaviour of U remains unknown, although experiments carried out on phosphogypsum, a waste by-product

generated from apatite in the production process of phosphoric acid and phosphate fertilizers, suggest that U uptake by gypsum is pH-controlled (Lin et al., 2018). Thus, the more alkaline the environment is, the higher the U concentration that could be expected in gypsum. However, the pH of evaporating seawater rarely reaches those values and tends to drop as the evaporation process goes on (Babel and Schreiber, 2014). Considering low salinity but high concentrations of  $\text{Ca}^{2+}$  and  $\text{SO}_4^{4-}$  (Clauer et al., 2000) during the formation of MSC evaporites, the alkalinity of the depositional environment might have increased. In any case, even the gypsum precipitated in U-rich environments like uranium mine tailings contains a high amount of Pb among other metals (Liu and Hendry, 2011).

The amount of common Pb is a challenge for dating young rocks, as their success strongly depends on the spread in the  $x$  axis ( $^{238}\text{U}/^{206}\text{Pb}$ ). In turn, given the same initial  $^{238}\text{U}/^{206}\text{Pb}$  ratio, older samples would have produced sufficient radiogenic Pb and thus a certain spread in the  $y$  axis ( $^{207}\text{Pb}/^{206}\text{Pb}$ ) as to be projected in a more precise regression line. Indeed, older samples are more influenced by the  $^{207}\text{Pb}/^{206}\text{Pb}$  ratio, and therefore it is highly likely that the success rate increases with the age of the sample.

#### 5.1.2 SC-ICPMS vs. MC-ICPMS

The first set of samples was measured with the SC-ICPMS. The U and Pb contents in the samples were rather low and produce large error ellipses in every single spot. This issue, together with low  $\mu$  ratios (i.e. spread on  $^{238}\text{U}/^{206}\text{Pb}$ ), produces substantial uncertainties in the final ages (Fig. 3) and a comparison with the depositional ages is poor. In order to achieve better results, we decided to accomplish subsequent measurements with the MC-ICPMS, which provides about 3 times better sensitivity and simultaneous isotope detection (Craig et al., 2018, 2020). The higher sensitivity implies smaller uncertainties in each spot, and hence more accurate and precise regression lines (i.e. ages) can be depicted.

Indeed, the improvement in age precision is clearly illustrated in Fig. 3. Although the results can be biased because fewer data were acquired during SC-ICPMS analyses, given a similar spread in the  $^{238}\text{U}/^{206}\text{Pb}$  axis, the uncertainties of ca. 15 % (MTO 11-3) and 20 % (MTO 4-4) obtained with the SC-ICPMS were reduced to 8 % (MTO 11-3, seq 2) and 11 % (MTO 4-4, seq 2) by using the MC-ICPMS (Fig. 3). Furthermore, the re-measurement of these two samples in another independent session in which higher  $^{238}\text{U}/^{206}\text{Pb}$  ratios were found reduced the uncertainties even more down to ca. 6 %.

### 5.2 U–Pb ages vs. cyclostratigraphic ages

Well-characterized matrix-matched reference material is essential for U–Pb analytical techniques using laser probes as matrix differences between the sample and reference standard can cause a significant offset in the obtained ages (Yang

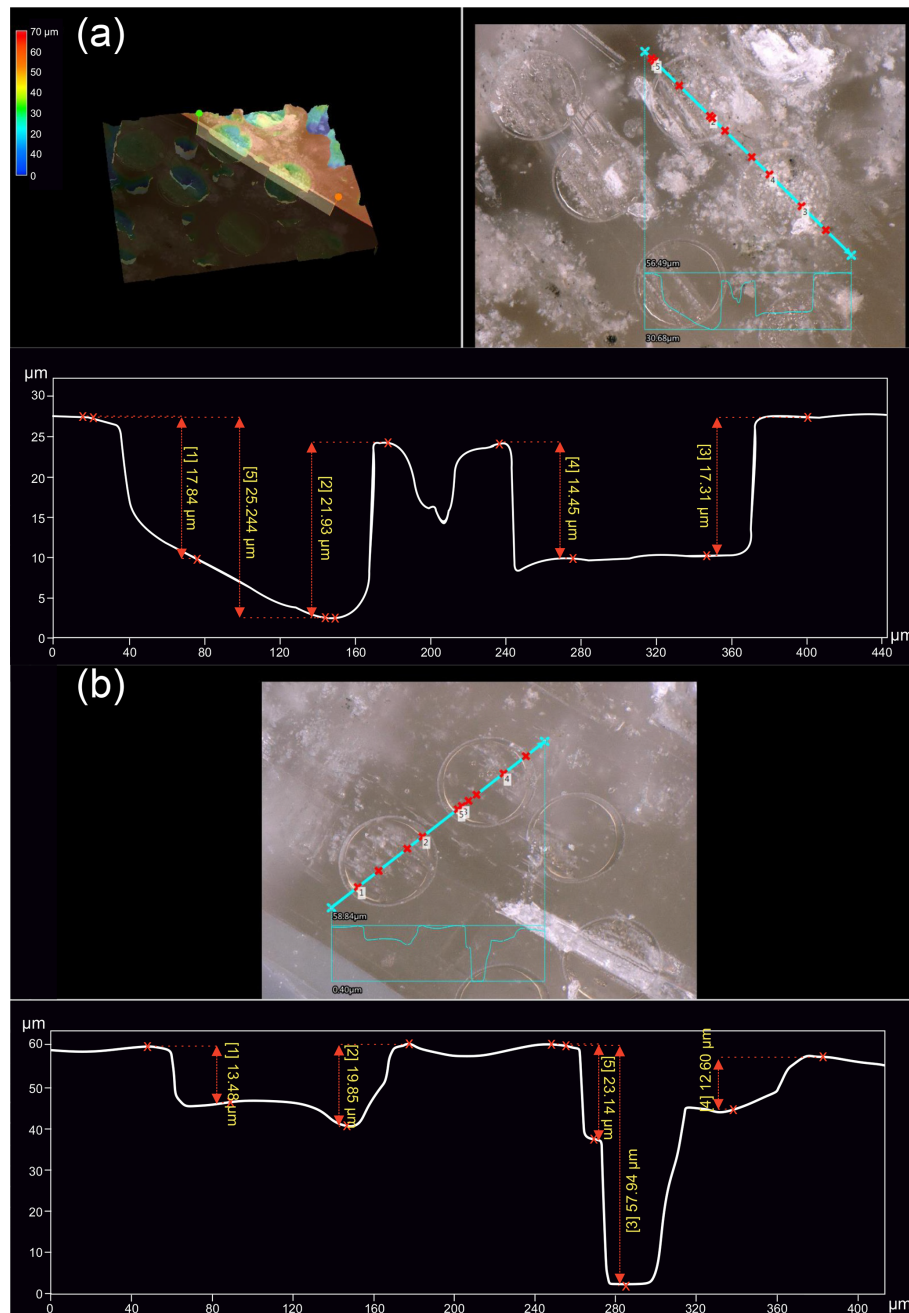


**Figure 4.** Pit depth profile of samples MTO 11-3 (a) and BCR 9644 (b). Whereas the pit shape is roughly homogeneous in MTO 11-3, sample BCR 9644 displays deeper areas in some of the pits. The profiles are measured using a Keyence digital microscope VHX-6000.

et al., 2018; Guillong et al., 2020). However, in the absence of sulfate reference materials, an attempt to use calcite reference materials was carried out, expecting that the offset between the two materials was going to be low or negligible. The light absorption observed in calcite and gypsum is similar, and they are easily ablated even at low fluence (less than  $2\text{ J cm}^{-2}$ ). As a comparison, Piccione et al. (2019) obtained analogous ages for contemporary fluorite and nacrite, both corrected to the same calcite reference material, even when

the fluorite has different light absorption and higher energy is needed for its ablation ( $5\text{--}6\text{ cm}^{-2}$ ). For those reasons, we expected a significantly lower matrix-induced offset than the one observed between calcite and zircon (4.7 %, Parrish et al., 2018).

The cyclostratigraphic ages of the MSC samples are well known (e.g. Vasilev et al., 2017) and we have used them for testing the suitability of the corrections with respect to carbonate matrix. As pointed out above, the majority of the

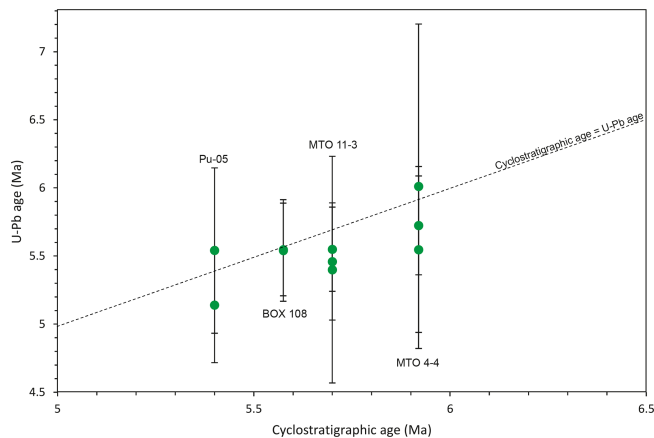


**Figure 5.** Comparison of the obtained U–Pb ages and the expected cyclostratigraphic ages. The weighted mean of the offsets between the two ages is  $-0.14 \pm 0.14$  Ma ( $\pm 2\sigma$ ). The dashed line represents the U–Pb age with the cyclostratigraphic age correlation.

samples contain a significant amount of common Pb, and only five ages were obtained. Although the  $\mu$  values of those samples were only moderate, the individual uncertainties range between 6 % and 11 %, and the ages obtained for samples MTO 4–4, MTO 11–3, Pu 05 and BOX 108 are in accordance with the cyclostratigraphic ages (e.g. Lugli et al., 2007; Vasiliev et al., 2017). A direct comparison of the U–Pb and cyclostratigraphic ages (Fig. 5), however, points to a slight bias toward younger ages, suggesting a systematic offset between the two. Taken singly, each U–Pb date overlaps the cyclostratigraphic age, but a more precise measure is the inverse-variance-weighted mean of all 10 discrepancies between the two ages. The calculated weighted average, i.e. the mean discrepancy, is  $-0.14 \pm 0.14$  Ma ( $\pm 2\sigma$ , MSWD = 0.77). This can now have both an analytical and a geological significance; it can be interpreted as (i) matrix mismatch between carbonate and sulfate or (ii) dating of a subsequent event instead of sedimentation. In fact, the mobilization of U and Pb during sediment compaction causes some U/Pb heterogeneity, which improves or enables the possibility of dating these sediments by the U–Pb method. The small mean age discrepancy obtained on the sulfate samples is in line with that reported from Montano et al. (2022) on lacustrine carbonates. In this study, although overlapping within uncertainties, a systematic offset was found between U–Pb ages of carbonate cement and that of zircon from ash layers. Thus, U–Pb ages of carbonate and sulfate cement likely date early diagenesis and not the sediment deposition. This supports our hypothesis that there is no difference in U–Pb fractionation between sulfate and carbonate matrix, although it is not direct evidence.

On the other hand, sample BCR 9644 resulted in an unexpected younger age of ca. 3 Ma. The brecciated nature of the sample, together with its extremely low Pb content ( $0.03 \mu\text{g g}^{-1}$  on average) in comparison with sur-

rounding samples, suggests a subsequent (re)crystallization and remobilization of U and Pb that could be related to the breccia formation. Warthmann et al. (2000) proposed important bacterial activity after the evaporite formation. For the equivalent-in-time Site 374, located south-east of Sicily, an approximately 3 m thick dolomitization front in Pliocene hemipelagic succession overlying the UG was identified. Here, a hypothesized role of the deep biosphere, sulfate-reducing bacteria thriving on the dissolution of sulfate-bearing minerals (Warthmann et al., 2000; Petrash et al., 2017) was suggested. Montano et al. (2019, 2021) showed that biological activity may control the U–Pb partitioning on carbonates, so the connection between the bacterial activity and the 3 Ma age could not be discarded. Although gypsum to anhydrite to gypsum (two-step) transformation can be considered another possible scenario, there is no observation in the literature that supports this hypothesis.

### 5.3 Pit depth profiles

Guillong et al. (2020) showed that different ablation parameters produce distinctive pit profiles (the so-called “aspect ratio” or depth to diameter ratio), and it could result in a noticeable bias in the data. The carbonate reference materials analysed here with a  $130 \mu\text{m}$  spot size resulted in a depth of ca.  $15 \mu\text{m}$  (aspect ratio of 0.12), whereas the sulfates vary between 16 and  $63 \mu\text{m}$  (aspect ratio between 0.12 and 0.48, Fig. 4). The ablation on NIST glass resulted in shallower ca.  $10 \mu\text{m}$  deep holes and an aspect ratio of 0.13, similar to the carbonates. This divergence between the sulfates could be attributed to various non-excluding features such as different textures, particle size, porosity or compaction (Elisha et al., 2021). However, in the cases with an aspect ratio mismatch relative to the primary standard of less than 2, a deviation lower than 5 % is anticipated (Guillong et al., 2020), which lies in the final result uncertainty of the majority of the samples analysed here. The larger discrepancy observed in sample Pu 05 (relative mismatch of 4) could result in age offsets up to 10 % (Guillong et al., 2020, their Fig. 4). However, Fig. 4b reveals an important heterogeneity in the pit profile in some samples, with a silhouette that resembles pores. Whether they correspond to porosity or chunks released due to a badly coupled laser beam, the signal remained stable.

These pit depth issues are also related to the downhole fractionation corrections. Mangenot et al. (2018) claimed that shallow pit depth compared to the spot size could minimize the downhole fractionation. That argument could apply to our reference materials and sulfates with shallower pit depth, but how it affects depths beyond 50–60  $\mu\text{m}$  can be arguable. Lenoir et al. (2021) obtained coherent regression lines in fluorites even with pit depths (up to 50 % variable) larger than spot sizes. Notwithstanding, the lack of bias between our U–Pb ages and cyclostratigraphic ages suggests

that the different downhole fractionation is not noticeable or remains within the uncertainties.

## 6 Conclusions

In this contribution, we have evaluated the applicability of carbonates as “almost-matrix-matched reference materials” for U–Pb dating of sulfates, and for that purpose, gypsum and anhydrite samples from the Messinian Salinity Crisis were analysed. The known cyclostratigraphic ages of these evaporites were compared with the in situ U–Pb ages obtained. The samples showed a high amount of common Pb and low spread in the U/Pb axis, and therefore only 15 % of the samples were successful. In fact, due to the large uncertainties obtained at the beginning, we were forced to switch from the SC-ICPMS to MC-ICPMS in order to improve the precision of the measurements. Four of the five successfully dated samples were indistinguishable within error from the expected ages, while the other was considerably younger. We assume that all the factors that could produce a bias in the final age, if any, are contained in the uncertainty, and therefore the use of carbonate reference materials could be a trustworthy approach for in situ U–Pb dating of sulfates. We acknowledge that the availability of sulfate reference material in the future will result in an improvement in both reliability and precision.

**Code and data availability.** The data have been processed with an in-house VBA spreadsheet programme (Gerdes and Zeh, 2006, <https://doi.org/10.1016/j.epsl.2006.06.039> and 2009, <https://doi.org/10.1016/j.chemgeo.2008.03.005>), which is available upon request.

All the raw data produced during this study are available in the Supplement.

**Supplement.** The supplement related to this article is available online at: <https://doi.org/10.5194/gchron-4-601-2022-supplement>.

**Author contributions.** AB and AG were involved in the LA-ICPMS analysis and pit depth measurements. IV accomplished the fieldwork and sample collection. All the authors collaborated in preparing the paper.

**Competing interests.** The contact author has declared that none of the authors has any competing interests.

**Disclaimer.** Publisher’s note: Copernicus Publications remains neutral with regard to jurisdictional claims in published maps and institutional affiliations.

**Acknowledgements.** This study has benefited greatly from insightful reviews by Andrew R. Kylander-Clark, Catherine Mottram and the associated editor Noah McLean, as well as the handling editor Klaus Mezger. This is FIERCE contribution no. 110. FIERCE is financially supported by the Wilhelm and Else Heraeus Foundation and by the Deutsche Forschungsgemeinschaft, which is gratefully acknowledged. Cores from borehole EMS-4 (Cattolica Eraclea) in the Caltanissetta Basin (Sicily) are stored in the core repository of the University of Milano, Department of Earth Science “Ardito Desio” after core restoration performed within COST Action CA15103 MEDSALT.

**Financial support.** This research has been supported by the post-doctoral fellowship programme, granted to the first author, of the Basque Government (grant no. POS\_2018\_1\_0018).

**Review statement.** This paper was edited by Noah M. McLean and reviewed by Andrew R. Kylander-Clark and Catherine Mottram.

## References

- Andreetto, F., Matsubara, K., Beets, C. J., Fortuin, A. R., Flecker, R., and Krijgsman, W.: High Mediterranean water-level during the Lago-Mare phase of the Messinian Salinity Crisis: insights from the Sr isotope records of Spanish marginal basins (SE Spain), *Paleogeogr. Paleoclimatol.*, 562, 110139, <https://doi.org/10.1016/j.palaeo.2020.110139>, 2021.
- Astilleros, J. M., Godelitsas, A., Rodríguez-Blanco, J. D., Fernández-Díaz, L., Prieto, M., Lagoyannis, A., and Harissopulos, S.: Interaction of gypsum with Pb – bearing aqueous solutions, *Appl. Geochem.*, 25, 1008–1016, <https://doi.org/10.1016/j.apgeochem.2010.04.007>, 2010.
- Babel, M. and Schreiber, B. C.: *Geochemistry of evaporites and evolution of seawater*, in: *Treatise on Geochemistry*, 2nd edn., edited by: Turekian, K. and Holland, H., Elsevier, Oxford, UK, 483–560, <https://doi.org/10.1016/B978-0-08-095975-7.00718-X>, 2014.
- Brannon, J. C., Cole, S. C., Podosek, F. A., Ragan, V. M., Coveney, R. M., Wallace, M. W., and Bradley, A. J.: Th–Pb and U–Pb dating of ore-stage calcite and Paleozoic fluid flow, *Science*, 271, 491–493, <https://doi.org/10.1126/science.271.5248.491>, 1996.
- Burisch, M., Walter, B. F., and Markl, G.: Silicification of Hydrothermal Gangue Minerals in Pb–Zn–Cu–Fluorite–Quartz–595 Baryte Veins, *Can. Mineral.*, 55, 501–514, <https://doi.org/10.3749/canmin.1700005>, 2017.
- Burisch, M., Gerdes, A., Meinert, L., Albert, R., Seifert, T., and Gutzmer, J.: The essence of time – fertile skarn formation in the Variscan Orogenic Belt, *Earth Planet. Sc. Lett.*, 519, 165–170, <https://doi.org/10.1016/j.epsl.2019.05.015>, 2019.
- CIESM: The Messinian salinity crisis from mega-deposits to microbiology, in: *A consensus report. 33ème CIESM Workshop Monographs 33*, edited by: Briand, F., CIESM Publisher, Monaco, 91–96, 2008.
- Clauer, N., Chaudhuri, S., Toulkeridis, T., and Blanc, G.: Fluctuations of Caspian Sea level: beyond climatic varia-

- tions?, *Geology*, 28, 1015–1018, [https://doi.org/10.1130/0091-7613\(2000\)28<1015:FOCSLB>2.0.CO;2](https://doi.org/10.1130/0091-7613(2000)28<1015:FOCSLB>2.0.CO;2), 2000.
- Conley, R. F. and Bundy, W. M.: Mechanism of gypsumification, *Geochim. Cosmochim. Ac.*, 15, 57–72, [https://doi.org/10.1016/0016-7037\(58\)90010-3](https://doi.org/10.1016/0016-7037(58)90010-3), 1958.
- Costanzo, A., Cipriani, M., Feely, M., Cianfione, G., and Dominici, R.: Messinian twinned selenite from the Catanzaro Trough, Calabria, Southern Italy: field, petrographic and fluid inclusion perspectives, *Carbonate. Evaporite.*, 34, 743–756, <https://doi.org/10.1007/s13146-019-00516-0>, 2019.
- Craig, G., Managh A. J., Stremtan, C., Lloyd, N. S., and Horstwood, M. S. A.: Doubling Sensitivity in Multicollector ICPMS Using High-Efficiency, Rapid Response Laser Ablation Technology, *Anal. Chem.*, 90, 11564–11571, <https://doi.org/10.1021/acs.analchem.8b02896>, 2018.
- Craig, G., Bracciali, L., and Lloyd, N.: LA-ICP-MS for U-(Th)-Pb geochronology: Which analytical capability is right for my laboratory?, *Thermo Fisher Scientific, Smart. Note* 30581, 2020.
- Cruset, D., Verges, J., Rodrigues, N., Belenguer, J., Pascual-Cebrian, E., Almar, Y., Perez-Caceres, I., Macchiavelli, C., Trave, A., Beranoaguirre, A., Albert, R., Gerdes, A., and Messenger, G.: U–Pb dating of carbonate veins constraining timing of beef growth and oil generation within Vaca Muerta Formation and compression history in the Neuquen Basin along the Andean fold and thrust belt, *Mar. Petrol. Geol.*, 132, 10520, <https://doi.org/10.1016/j.marpetgeo.2021.105204>, 2021.
- Deng, X. D., Li, J. W., Luo, T., and Wang, H. Q.: Dating magmatic and hydrothermal processes using andradite-rich garnet U–Pb geochronometry, *Contrib. Mineral. Petr.*, 172, 71, <https://doi.org/10.1007/s00410-017-1389-2>, 2017.
- Elisha, B., Nuriel, P., Kylander-Clark, A., and Weinberger, R.: Towards in situ U–Pb dating of dolomite, *Geochronology*, 3, 337–349, <https://doi.org/10.5194/gchron-3-337-2021>, 2021.
- Evans, N. P., Turchyn, A. V., Gázquez, F., Bontognali, R. R., Chapman, H. J., and Hodell, D. A.: Coupled measurements of  $\delta^{18}\text{O}$  and  $\delta\text{D}$  of hydration water and salinity of fluid inclusions in gypsum from the Messinian Yesares Member, Sorbas Basin (SE Spain), *Earth Planet. Sc. Lett.*, 430, 499–510, <https://doi.org/10.1016/j.epsl.2015.07.071>, 2015.
- Flecker, R. and Ellam, R. M.: Identifying Late Miocene episodes of connection and isolation in the Mediterranean–Paratethyan realm using Sr isotopes, *Sediment. Geol.*, 188–189, 189–203, <https://doi.org/10.1016/j.sedgeo.2006.03.005>, 2006.
- Flecker, R., Krijgsman, W., Capella, W., de Castro Martins, C., Dmitrieva, E., Mayser, J. P., Marzocchi, A., Modestu, S., Lozano, D. O., Simon, D., Tulbure, M., van den Berg, B., van der Schee, M., de Lange, G., Ellam, R., Govers, R., Gutjahr, M., Hilgen, F., Kouwenhoven, T., Lofi, J., Meijer, P., Sierro, F. J., Bachiri, N., Barhoun, N., Alami, A. C., Chacon, B., Flores, Jose A., Gregory, J., Howard, J., Lunt, D., Ochoa, M., Pancost, R., Vincent, S., and Yousfi, M. Z.: Evolution of the Late Miocene Mediterranean Atlantic gateways and their impact on regional and global environmental change, *Earth-Sci. Rev.*, 150, 365–392, <https://doi.org/10.1016/j.earscirev.2015.08.007>, 2015.
- Gerdes, A. and Zeh, A.: Combined U–Pb and Hf isotope LA-(MC-)ICP-MS analyses of detrital zircons: comparison with SHRIMP and new constraints for the provenance and age of an Armorican metasediment in Central Germany, *Earth Planet. Sc. Lett.*, 249, 47–61, <https://doi.org/10.1016/j.epsl.2006.06.039>, 2006.
- Gerdes, A. and Zeh, A.: Zircon formation versus zircon alteration – new insights from combined U–Pb and Lu–Hf in-situ LA-ICP-MS analyses, and consequences for the interpretation of Archean zircon from the Central Zone of the Limpopo Belt, *Chem. Geol.*, 261, 230–243, <https://doi.org/10.1016/j.chemgeo.2008.03.005>, 2009.
- Grandia, F., Asmerom, Y., Getty, S., Cardellach, E., and Canals, A.: U–Pb dating of MVT ore-stage calcite: implications for fluid flow in a Mesozoic extensional basin from Iberian Peninsula, *J. Geochem. Explor.*, 69, 377–380, [https://doi.org/10.1016/S0375-6742\(00\)00030-3](https://doi.org/10.1016/S0375-6742(00)00030-3), 2000.
- Grothe, A., Andreetto, F., Reichart, G. J., Wolthers, M., Van Baak, C. G., Vasiliev, I., Stoica, M., Sangiorgi, F., Middelburg, J. J., Davies, G. R., and Krijgsman, W.: Paratethys pacing of the Messinian Salinity Crisis: low salinity waters contributing to gypsum precipitation?, *Earth Planet. Sc. Lett.*, 532, 116029, <https://doi.org/10.1016/j.epsl.2019.116029>, 2020.
- Guillong, M., Wotzlaw, J.-F., Looser, N., and Laurent, O.: Evaluating the reliability of U–Pb laser ablation inductively coupled plasma mass spectrometry (LA-ICP-MS) carbonate geochronology: matrix issues and a potential calcite validation reference material, *Geochronology*, 2, 155–167, <https://doi.org/10.5194/gchron-2-155-2020>, 2020.
- Horstwood, M. S. A., Košler, J., Gehrels, G., Jackson, S. E., McLean, N. M., Paton, C., Pearson, N. J., Sircombe, K., Sylvester, P., Vermeesch, P., and Bowring, J. F.: Community-derived standards for LA-ICP-MS U-(Th)-Pb geochronology-Uncertainty propagation, age interpretation and data reporting, *Geostand. Geoanal. Res.*, 40, 311–332, <https://doi.org/10.1111/j.1751-908X.2016.00379.x>, 2016.
- Hsü, K. J., Ryan, W. B. F., and Cita, M. B.: Late Miocene desiccation of the Mediterranean, *Nature*, 242, 240–244, <https://doi.org/10.1038/242240a0>, 1973.
- Hsü, K. J., Montadert, L., Ross, D. A., and Neprochnov, Y. P.: Annotated record of the detailed examination of Mn deposits from DSDP Leg 42 (Holes 372 and 379A), *Pangaea [data set]*, <https://doi.org/10.1594/PANGAEA.871889>, 1978.
- Jochum, K. P., Weis, U., Stoll, B., Kuzmin, D., Yang, Q., Raczek, I., Jacob, D. E., Stracke, A., Birbaum, K., Frick, D. A., Günther, D., and Enzweiler, J.: Determination of reference values for NIST SRM 610–617 glasses following ISO guidelines, *Geostand. Geoanal. Res.*, 35, 97–429, <https://doi.org/10.1111/j.1751-908X.2011.00120.x>, 2011.
- Kameda, K., Hashimoto, Y., Wang, S.-L., Hirai, Y., and Miyahara, H.: Simultaneous and continuous stabilization of As and Pb in contaminated solution and soil by a ferrihydrite-gypsum sorbent, *J. Hazard. Mater.*, 327, 171–179, <https://doi.org/10.1016/j.jhazmat.2016.12.039>, 2017.
- Krijgsman, W., Hilgen, F. J., Raffi, I., Sierro, F. J., and Wilson, D. S.: Chronology, causes and progression of the Messinian Salinity Crisis, *Nature*, 400, 652–655, <https://doi.org/10.1038/23231>, 1999.
- Krijgsman, W., Stoica, M., Vasiliev, I., and Popov, V. V.: Rise and fall of the Paratethys Sea during the Messinian Salinity Crisis, *Earth Planet. Sc. Lett.*, 290, 183–191, <https://doi.org/10.1016/j.epsl.2009.12.020>, 2010.
- Krijgsman, W., Capella, W., Simon, D., Hilgen, F. J., Kouwenhoven, T. J., Meijer, P. T., Sierro, F. J., Tulbure, M. A., van den Berg, B. C. J., van der Schee, M., and Flecker, R.: The Gibraltar

- Corridor: watergate of the Messinian Salinity Crisis, *Mar. Geol.*, 403, 238–246, <https://doi.org/10.1016/j.margeo.2018.06.008>, 2018.
- Laskar, J.: The limits of Earth orbital calculations for geological time-scale use, in: *Astronomical (Milankovitch) Calibration of the Geological Time-Scale*, edited by: Shackleton, N. J., McCave, I. N., and Graham, P. W., *Philos. T. Roy. Soc. A.*, 357, 1735–1759, <https://doi.org/10.1098/rsta.1999.0399>, 1999.
- Lenoir, L., Blaise, T., Somogyi, A., Brigaud, B., Barbarand, J., Boukari, C., Nouet, J., Brézard-Oudot, A., and Pagel, M.: Uranium incorporation in fluorite and exploration of U–Pb dating, *Geochronology*, 3, 199–227, <https://doi.org/10.5194/gchron-3-199-2021>, 2021.
- Lin, J., Sun, W., Desmarais, J., Chen, N., Feng, R., Zhang, P., Li, D., Lieu, A., Tse, J. S., and Pan, Y.: Uptake and speciation of uranium in synthetic gypsum ( $\text{CaSO}_4 \cdot 2\text{H}_2\text{O}$ ): applications to radioactive mine tailings, *J. Environ. Radioactiv.*, 181, 8–17, <https://doi.org/10.1016/j.jenvrad.2017.10.010>, 2018.
- Liu, D. J. and Hendry, M. J.: Controls on  $^{226}\text{Ra}$  during raffinate neutralization at the Key Lake uranium mill, Saskatchewan, Canada, *Appl. Geochem.*, 26, 2113–2120, <https://doi.org/10.1016/j.apgeochem.2011.07.009>, 2011.
- Ludwig, K. R.: *User's Manual for Isoplot Version 3.75-4.15: a Geochronological Toolkit for Microsoft Excel*, Berkeley Geochronological Center Special Publication, no. 5, 2012.
- Lugli, S., Bassetti, M. A., Manzi, V., Barbieri, M., Longinelli, A., and Roveri, M.: The Messinian “Vena del Gesso” evaporites revisited: characterization of isotopic composition and organic matter, *J. Geol. Soc. Lond.*, 285, 179–190, <https://doi.org/10.1144/SP285.11>, 2007.
- Lugli, S., Manzi, V., Roveri, M., and Schreiber, B. C.: The primary Lower Gypsum in the Mediterranean: a new facies interpretation for the first stage of the Messinian salinity crisis, *Palaeogeogr. Palaeoclimatol.*, 297, 83–99, <https://doi.org/10.1016/j.palaeo.2010.07.017>, 2010.
- Mangenot, X., Gasparrini, M., Rouchon, V., and Bonifacie, M.: Basin-scale thermal and fluid flow histories revealed by carbonate clumped isotopes ( $\Delta 47$ ) – Middle Jurassic carbonates of the Paris Basin decopentrate, *Sedimentology*, 65, 123–150, <https://doi.org/10.1111/sed.12427>, 2018.
- Manzi, V., Gennari, R., Lugli, S., Roveri, M., and Schreiber, B. C.: The Messinian “Calcare di Base” (Sicily, Italy) revisited, *Geol. Soc. Am. Bull.*, 123, 347–370, <https://doi.org/10.1130/B30262.1>, 2011.
- Manzi, V., Gennari, R., Hilgen, F., Krijgsman, W., Lugli, S., Roveri, M., and Sierro, F. J.: Age refinement of the Messinian salinity crisis onset in the Mediterranean, *Terra Nova*, 25, 315–322, <https://doi.org/10.1111/ter.12038>, 2013.
- Manzi, V., Gennari, R., Lugli, S., Persico, D., Reghizzi, M., Roveri, M., Schreiber, B. C., Calvo, R., Gavrieli, I., and Gvirtzman, Z.: The onset of the Messinian salinity crisis in the deep Eastern Mediterranean basin, *Terra Nova*, 30, 189–198, <https://doi.org/10.1111/ter.12325>, 2018.
- Meilijson, A., Hilgen, F., Sepúlveda, J., Steinberg, J., Fairbank, V., Flecker, R., Waldmann, N. D., Spaulding, S. A., Bialik, O. M., and Boudinot, F. G.: Chronology with a pinch of salt: integrated stratigraphy of Messinian evaporites in the deep Eastern Mediterranean reveals long-lasting halite deposition during Atlantic connectivity, *Earth-Sci. Rev.*, 194, 374–398, <https://doi.org/10.1016/j.earscirev.2019.05.011>, 2019.
- Millonig, L. J., Albert, R., Gerdes, A., Avigad, D., and Dietsch, C.: Exploring laser ablation U–Pb dating of regional metamorphic garnet – The Straits Schist, Connecticut, USA, *Earth Planet. Sc. Lett.*, 552, 116589, <https://doi.org/10.1016/j.epsl.2020.116589>, 2020.
- Montano, D., Gasparrini, M., Gerdes, A., Albert, R., Rohais, S., and Della Porta, G.: In-situ carbonate U–Pb analysis by LA-ICP-MS: From absolute dating to understanding the U–Pb partitioning in lacustrine systems, *Goldschmidt 2019 Abstracts*, Abstract no. 2323, 2019.
- Montano, D., Gasparrini, M., Gerdes, A., Della Porta, G., and Albert, R.: In-situ U–Pb dating of Ries Crater lacustrine carbonates (Miocene, South-West Germany): implications for continental carbonate chronostratigraphy, *Earth Planet. Sc. Lett.*, 568, 117011, <https://doi.org/10.1016/j.epsl.2021.117011>, 2021.
- Montano, D., Gasparrini, M., Rohais, S., Albert, R., and Gerdes, A.: Depositional age models in lacustrine systems from zircon and carbonate U–Pb geochronology, *Sedimentology*, in press, <https://doi.org/10.1111/sed.13000>, 2022.
- Morales, J., Astilleros, J. M., Jiménez, A., Göttlicher, J., Steininger, R., and Fernández-Díaz, L.: Uptake of dissolved lead by anhydrite surfaces, *Appl. Geochem.*, 40, 89–96, <https://doi.org/10.1016/j.apgeochem.2013.11.002>, 2014.
- Murray, R. C.: Origin and diagenesis of gypsum and anhydrite, *SEPM Journal of Sedimentary Research*, 34, 512–523, <https://doi.org/10.1306/74D710D2-2B21-11D7-8648000102C1865D>, 1964.
- Natalicchio, M., Dela Pierre, F., Lugli, S., Lowenstein, T. K., Feiner, S. J., Ferrando, S., Manzi, V., Roveri, M., and Clari, P.: Did Late Miocene (Messinian) gypsum precipitate from evaporated marine brines? Insights from the Piedmont Basin (Italy), *Geology*, 42, 179–182, <https://doi.org/10.1130/G34986.1>, 2014.
- Nuriel, P., Wotzlaw, J.-F., Ovtcharova, M., Vaks, A., Stremtan, C., Šála, M., Roberts, N. M. W., and Kylander-Clark, A. R. C.: The use of ASH-15 flowstone as a matrix-matched reference material for laser-ablation U–Pb geochronology of calcite, *Geochronology*, 3, 35–47, <https://doi.org/10.5194/gchron-3-35-2021>, 2021.
- Ossorio, M., Van Driessche, A. E. S., Pérez, P., and García-Ruiz, J. M.: The gypsum-anhydrite paradox revisited, *Chem. Geol.*, 386, 16–21, <https://doi.org/10.1016/j.chemgeo.2014.07.026>, 2014.
- Pagel, M., Bonifacie, M., Schneider, D. A., Gautheron, C., Brigaud, B., Calmels, D., Cros, A., Saint-Bezar, B., Landrein, P., Sutcliffe, C., and Davis, D.: Improving paleohydrological and diagenetic reconstructions in calcite veins and breccia of a sedimentary basin by combining  $\Delta 47$  temperature,  $\delta^{18}\text{O}$  water and U–Pb age, *Chem. Geol.*, 481, 1–17, <https://doi.org/10.1016/j.chemgeo.2017.12.026>, 2018.
- Parrish, R. R., Parrish, C. M., and Lasalle, S.: Vein calcite dating reveals Pyrenean orogen as cause of Paleogene deformation in southern England, *J. Geol. Soc.*, 175, 425–442, <https://doi.org/10.1144/jgs2017-107>, 2018.
- Petrash, D. A., Bialik, O. M., Bontognali, T. R. R., Vasconcelos, C., Roberts, J. A., McKenzie, J. A., and Konhauser, K. O.: Microbially catalyzed dolomite formation: From near-surface to burial, *Earth-Sci. Rev.*, 171, 558–582, <https://doi.org/10.1016/j.earscirev.2017.06.015>, 2017.

- Piccione, G., Rasbury, E. T., Elliott, B. A., Kyle, J. R., Jaret, S. J., Acerbo, A. S., Lanzirrotti, A., Northrup, P., Wooton, K., and Parrish, R. R.: Vein fluorite U–Pb dating demonstrates post-6.2 Ma rare-earth element mobilization associated with Rio Grande rifting, *Geosphere*, 15, 1958–1972, <https://doi.org/10.1130/GES02139.1>, 2019.
- Rasbury, E. T. and Cole, J. M.: Directly dating geologic events: U–Pb dating of carbonates, *Reviews of Geophysics*, 47, RG3001, <https://doi.org/10.1029/2007RG000246>, 2009.
- Ring, U. and Gerdes, A.: Kinematics of the Alpenrhein-Bodensee graben system in the Central Alps: Oligocene/Miocene transtension due to formation of the Western Alps arc, *Tectonics*, 35, 1367–1391, <https://doi.org/10.1002/2015TC004085>, 2016.
- Roberts, N. M. W., Rasbury, E. T., Parrish, R. R., Smith, C. J., Horstwood, M. S. A., and Condon, D. J.: A calcite reference material for LA-ICP-MS U–Pb geochronology, *Geochem. Geophys. Geos.*, 18, 2807–2814, <https://doi.org/10.1002/2016GC006784>, 2017.
- Roberts, N. M. W., Drost, K., Horstwood, M. S. A., Condon, D. J., Chew, D., Drake, H., Milodowski, A. E., McLean, N. M., Smye, A. J., Walker, R. J., Haslam, R., Hodson, K., Imber, J., Beaudoin, N., and Lee, J. K.: Laser ablation inductively coupled plasma mass spectrometry (LA-ICP-MS) U–Pb carbonate geochronology: strategies, progress, and limitations, *Geochronology*, 2, 33–61, <https://doi.org/10.5194/gchron-2-33-2020>, 2020.
- Rouchy, J. M. and Caruso, A.: The Messinian salinity crisis in the Mediterranean basin: a reassessment of the data and an integrated scenario, *Sediment. Geol.*, 188–189, 35–67, <https://doi.org/10.1016/j.sedgeo.2006.02.005>, 2006.
- Roveri, M., Lugli, S., Manzi, V., and Schreiber, B. C.: The Messinian Sicilian stratigraphy revisited: toward a new scenario for the Messinian salinity crisis, *Terra Nova*, 20, 483–488, <https://doi.org/10.1111/j.1365-3121.2008.00842.x>, 2008a.
- Roveri, M., Bertini, A., Cosentino, D., Di Stefano, A., Gennari, R., Gliozzi, E., Grossi, F., Iaccarino, S. M., Lugli, S., Manzi, V., and Taviani, M.: A high-resolution stratigraphic framework for the latest Messinian events in the Mediterranean area, *Stratigraphy*, 5, 323–342, 2008b.
- Roveri, M., Flecker, R., Krijgsman, W., Lofi, J., Lugli, S., Manzi, V., Sierro, F. J., Bertini, A., Camerlenghi, A., De Lange, G., Govers, R., Hilgen, F. J., Hübscher, C., Meijer, P. T., and Stouica, M.: The Messinian Salinity Crisis: past and future of a great challenge for marine sciences, *Mar. Geol.*, 352, 25–58, <https://doi.org/10.1016/j.margeo.2014.02.002>, 2014a.
- Roveri, M., Lugli, S., Manzi, V., Gennari, R., and Schreiber, B. C.: High-resolution strontium isotope stratigraphy of the Messinian deep Mediterranean basins: implications for marginal to central basins correlation, *Mar. Geol.*, 349, 113–125, <https://doi.org/10.1016/j.margeo.2014.01.002>, 2014b.
- Ryan, W. B.: Decoding the Mediterranean salinity crisis, *Sedimentology*, 56, 95–136, <https://doi.org/10.1111/j.1365-3091.2008.01031.x>, 2009.
- Schaltegger, U., Schmitt, A. K., and Horstwood, M. S. A.: U–Th–Pb zircon geochronology by ID-TIMS, SIMS, and laser ablation ICP-MS: Recipes, interpretations, and opportunities, *Chem. Geol.*, 402, 89–110, <https://doi.org/10.1016/j.chemgeo.2015.02.028>, 2015.
- Selli, R.: Il Messiniano Mayer-Eymar 1867. Proposta di un neostratotipo, *Giornale di Geologia*, 28, 1–33, 1960.
- Seman, S., Stockli, D. F., and McLean, N. M.: U–Pb geochronology of grossular-andradite garnet, *Chem. Geol.*, 460, 106–116, <https://doi.org/10.1016/j.chemgeo.2017.04.020>, 2017.
- Sindern, S., Havenith, V., Gerdes, A., Meyer, F. M., Adelman, D., and Hellmann, A.: Dating of anatase-forming diagenetic reactions in Rotliegend sandstones of the North German Basin, *Int. J. Earth Sci.*, 108, 1275–1292, <https://doi.org/10.1007/s00531-019-01705-x>, 2019.
- Sylvester, P. (Ed.): Matrix effects in Laser ablation-ICP-MS, in: *Laser Ablation-ICP-MS in the Earth Sciences: Current Practices and Outstanding Issues*, Mineralogical association of Canada, 67–78, 2008.
- Van Driessche, A. E. S., Stawski, T., and Kellermeier, M.: Calcium sulfate precipitation pathways in natural and engineering environments, *Chem. Geol.*, 530, 119274, <https://doi.org/10.1016/j.chemgeo.2019.119274>, 2019.
- Vasiliev, I., Mezger, E. M., Lugli, S., Reichart, G. J., Manzi, V., and Roveri, M.: How dry was the Mediterranean during the Messinian salinity crisis?, *Paleogeogr. Paleoclimatol.*, 471, 120–133, <https://doi.org/10.1016/j.palaeo.2017.01.032>, 2017.
- Wafforn, S., Seman, S., Kyle, J. R., Stockli, D., Leys, C., Sonbait, D., and Cloos, M.: Andradite garnet U–Pb geochronology of the big Gossan skarn, Ertzberg-Grasberg mining district, Indonesia, *Econ. Geol.*, 113, 769–778, <https://doi.org/10.5382/econgeo.2018.4569>, 2018.
- Warren, J. K.: *Evaporites: A Geological Compendium*, Springer, Berlin, <https://doi.org/10.1007/978-3-319-13512-0>, 2016.
- Warthmann, R., van Lith, Y., Vasconcelos, C., McKenzie, J. A., and Karpoff, A. M.: Bacterially induced dolomite precipitation in anoxic culture experiments, *Geology*, 28, 1091–1094, [https://doi.org/10.1130/0091-7613\(2000\)28<1091:BIDPIA>2.0.CO;2](https://doi.org/10.1130/0091-7613(2000)28<1091:BIDPIA>2.0.CO;2), 2000.
- Woodhead, J., Hellstrom, J., Maas, R., Drysdale, R., Zanchetta, G., Devine, P., and Taylor, E.: U–Pb geochronology of speleothems by MC-ICPMS, *Quat. Geochronol.*, 1, 208–221, <https://doi.org/10.1016/j.quageo.2006.08.002>, 2006.
- Woodhead, J., Hellstrom, J., Pickering, R., Drysdale, R., Paul, B., and Bajo, P.: U and Pb variability in older speleothems and strategies for their chronology, *Quat. Geochronol.*, 14, 105–113, <https://doi.org/10.1016/j.quageo.2012.02.028>, 2012.
- Yan, S., Zhou, R. J., Niu, H. C., Feng, Y. X., Nguyen, A. D., Zhao, Z. H., Yang, W. B., Qian, D., and Zhao, J. X.: LA-MC-ICP-MS U–Pb dating of low-U garnets reveals multiple episodes of skarn formation in the volcanic-hosted iron mineralization system, Awulale belt, Central Asia, *Geol. Soc. Am. Bull.*, 132, 1031–1045, <https://doi.org/10.1130/B35214.1>, 2020.
- Yang, Y. H., Wu, F. Y., Yang, J. H., Mitchell, R. H., Zhao, Z. F., Xie, L. W., Huang, C., Ma, Q., Yang, M., and Zhao, H.: U–Pb age determination of schorlomite garnet by laser ablation inductively coupled plasma mass spectrometry, *J. Anal. Atom. Spectrom.*, 33, 231–239, <https://doi.org/10.1039/c7ja00315c>, 2018.
- Zachariasse, W. J., van Hinsbergen, D. J. J., and Fortuin, A. R.: Mass wasting and uplift on Crete and Karpathos during the early Pliocene related to initiation of south Aegean left-lateral, strike-slip tectonics, *Geol. Soc. Am. Bull.*, 120, 976–993, <https://doi.org/10.1130/B26175.1>, 2008.